BPR MCS
Bulletin of Pioneering Researches of Medical and Clinical Science

Bulletin of Pioneering Researches of Medical and Clinical Science

Available online: https://bprmcs.com
2024 | Volume 4 | Issue 2 | Page: 186-202

Inhibition of TNF-α/NF-κB Signaling Underlies the Protective Effect of Gypenosides Against CORT-Induced Ferroptosis in PC12 Cells

Ahmed Mansour[1]*, Omar Saeed[1]

[1]Department of Medical and Clinical Research, Cairo University, Cairo, Egypt.

Abstract

Persistent psychological strain may trigger malfunction of the nervous system, together with behaviors resembling depression in animals. Gypenosides can relieve neuronal damage caused by sustained stress, though the protective pathway remains inadequately characterized. The current work set out to probe the influence and operational mechanisms of gypenosides on neuronal ferroptosis induced by chronic stress. To this end, an in vitro model of sustained stress-induced neuronal impairment was created by applying corticosterone to induce injury in PC12 cells. We established that the ferroptosis blockers DFO and Ferrostatin-1 reduced corticosterone-driven cell death in PC12 cells by lowering iron deposition and lipid peroxidation and by boosting cellular survival. At the same time, gypenosides lessened ferroptosis induced by the ferroptosis inducer Erastin in PC12 cells. Subsequently, gypenosides prevented corticosterone-elicited ferroptosis in PC12 cells. At the molecular level, gypenosides reduced the abundance of Hepcidin and DMT1 and increased the abundance of Ferritin and FPN1, thereby restoring the corticosterone-disturbed iron equilibrium and alleviating iron overload. In parallel, gypenosides alleviated corticosterone-driven lipid peroxidation by restraining GLS2 expression, increasing SLC7A11 and glutathione peroxidase 4 levels, and curtailing glutamate accumulation and GSH exhaustion. Gypenosides also reduced corticosterone-induced secretion of inflammatory mediators, TNFR1 levels, and NF-κB and p53 phosphorylation in PC12 cells. Altogether, these results imply that gypenosides ease corticosterone-elicited ferroptosis via suppressing the TNF-α/NF-κB signaling cascade in PC12 cells.

Keywords: Gypenosides, Ferroptosis, Chronic stress, Lipid peroxidation, Iron homeostasis

Corresponding author: Ahmed Mansour
E-mail: ahmed.mansour@gmail.com

How to Cite This Article: Mansour A, Saeed O. Inhibition of TNF-α/NF-κB Signaling Underlies the Protective Effect of Gypenosides Against CORT-Induced Ferroptosis in PC12 Cells. Bull Pioneer Res Med Clin Sci. 2024;4(2):186-202. https://doi.org/10.51847/nBFetxR4X2

Introduction

In veterinary medicine, prolonged stress can disrupt the nervous system, leading to failures in multiple organ systems and atypical behavior in chickens, dogs, pigs, and other animals. Investigations have revealed that sustained stress can elicit deviant behaviors, including reduced feeding, repetitive chewing, and tail biting in pigs [1, 2]. As a consequence, unremitting stress reduces feed intake, feed conversion efficiency, productive output, and commodity quality in animals, causing varying degrees of financial harm to the livestock sector. Evidence indicates that prolonged stress can overstimulate the hypothalamic-pituitary-adrenal (HPA) axis, leading to anomalous surges in glucocorticoids and culminating in neuronal injury and depression-mimicking behavior in animals [3, 4]. Ongoing stress can lead to aberrant HPA axis activation, elevated corticosterone (CORT) levels, and reduced hippocampal neuron density, resulting in depressive-like behavior in

This work is licensed under the Creative Commons Attribution 4.0 International License.

pigs [1]. Still, the disease's origin and the molecular circuits underlying neuronal impairment caused by persistent stress warrant deeper exploration.

Ferroptosis represents a newly recognized mode of programmed cell death characterized by the accumulation of substantial iron-dependent lipid peroxides (LPO) and reactive oxygen species (ROS) [5, 6]. Selective blockers, such as Ferrostatin-1 and the iron-scavenging agent deferoxamine (DFO), can inhibit ferroptosis [5]. Our earlier investigation showed that Ferrostatin-1 and DFO prevented cell death by reducing iron accumulation and LPO in microglia [7]. Present-day knowledge indicates that multiple biological phenomena are tightly linked to ferroptosis, including inflammatory reactions, disturbances in iron homeostasis, glutathione (GSH) deficiency, and the inactivation of Glutathione Peroxidase 4 (GPX4), which together lead to the accumulation of LPO and ROS and eventual cell death [8, 9]. A balanced iron state is indispensable for the persistence of nerve cells [10]. Prior studies have indicated that prolonged stress can trigger neural inflammation, which dysregulates iron-handling proteins and leads to iron overload in nerve cells [11, 12]. The collapse of iron homeostasis triggers extreme LPO accumulation, a key characteristic of ferroptosis [9]. Beyond this, unyielding stress can disrupt glutamate signaling in the brain, leading to excitotoxic injury and additional neuronal degeneration [13, 14]. Persistent stress can concurrently increase serum CORT and nitric oxide levels while reducing neurotransmitter synthesis, possibly triggering abnormal behavior in pigs [15]. Our own prior work demonstrates that sustained stress worsens nano-aluminum particle-triggered ferroptosis within hippocampal neurons of rats [11]. It follows that blocking neuronal ferroptosis could serve as a remedial avenue to alleviate the neuronal damage associated with chronic stress. Even so, further inquiry is essential to identify treatment candidates and clarify the exact safeguarding processes.

Gypenosides (GPs), an assembly of tetracyclic or pentacyclic triterpenoid saponins extracted from Gynostemma pentaphyllum, bear structural likeness to certain ginsenosides yet manifest a unique bioactive fingerprint [16]. Gypenosides have been reported to possess antioxidant, neuroprotective, anti-inflammatory, and mood-lifting properties [17, 18]. They may be employed both as botanical feed supplements for farm animals and poultry to stimulate growth and improve product standards, and as medicinal preparations to help prevent and control ailments in livestock and poultry. Published work has shown that GPs can significantly modulate the release of inflammatory mediators, raise GSH levels, and curb the generation of LPO and ROS, thereby reducing oxidative injury in rats subjected to chronic cerebral blood flow reduction [19]. Recent findings indicate that gypenoside A mitigates retinal microvascular impairment induced by high glucose by suppressing ferroptosis [16]. Nonetheless, the defensive consequences and mechanisms of GPs on neuronal ferroptosis induced by ongoing stress remain to be unraveled.

The signaling proteins interleukin (IL)-6 and tumor necrosis factor (TNF)-α can disrupt iron metabolism by activating nuclear factor kappa B (NF-κB) [9]. Both TNF-α and NF-κB are candidate molecular targets for therapeutic intervention in neuronal injury [20, 21]. The TNF-α/NF-κB signaling pathway occupies multiple central positions in regulating neuronal injury mediated by programmed cell death [21, 22]. Triggering the TNF-α/NF-κB axis can boost Hepcidin production, which, in turn, raises DMT1 levels and lowers FPN1 levels [23]. Moreover, NF-κB activation is a prerequisite for neuronal ferroptosis [24]. TNF-α-stimulated NF-κB can switch on the tumor suppressor p53, a factor of major importance in controlling ferroptosis [9]. In addition, p53 can disrupt glutamate (Glu) handling and lead to a GSH deficiency, a chain of events culminating in ferroptotic death of neurons [25]. Earlier work documented that GPs can suppress NF-κB activation and reduce the production of the inflammatory cytokines IL-6, IL-1β, and TNF-α. These outcomes together ease chronic stress-driven hippocampal neuroinflammation and behavioral signs of depression in rats [18]. What remains unresolved, however, is whether GPs put the brakes on chronic stress-induced neuronal ferroptosis via the TNF-α/NF-κB signaling axis.

Hyperactivation of the HPA axis is a defining hallmark of the chronic stress response, and CORT is routinely used to establish in vitro models of chronic stress [26]. PC12 cells, derived from rat pheochromocytoma, are widely used across neuroscience disciplines, including studies of neurotoxicity, neuroinflammation, and neuroprotection [27]. For these reasons, we applied CORT to induce damage in PC12 cells, thereby replicating an in vitro model of neuronal injury under chronic stress. Specific ferroptosis antagonists, Ferrostatin-1 and DFO, were used to determine whether CORT induced ferroptosis in PC12 cells. Next, the specific ferroptosis agonist Erastin was used to assess the protective effect of GPs on ferroptosis in PC12 cells. In the final step, PC12 cells were pre-exposed to GPs to probe whether GPs could reverse CORT-evoked ferroptosis in PC12 cells through dampening the TNF-α/NF-κB signaling cascade. The present investigation supplies a conceptual and experimental platform for deploying GPs to forestall and manage stress states in animals. At the same time, it identifies druggable targets for sifting anti-stress compounds in livestock production settings.

Materials and Methods

Cell culture and drug treatments

PC12 cells were procured from the Henan Engineering Technology Research Center of Industrial Microbial Strains. The cells were propagated in DMEM (Dulbecco's Modified Eagle Medium) from Gibco (Thermo, Waltham, MA, USA), enriched with 10% fetal bovine serum (FBS, BI, Beit Haemek, Israel) and 100 U/mL penicillin-streptomycin. Cultures were sustained at 37 °C in a humidified atmosphere (Thermo, Waltham, MA, USA) with 5% CO_2. Cells were expanded to 70–80% confluence in T25 flasks. Before treatment, PC12 cells were dispensed at 5 × 10^3 cells/mL into 6-well or 96-well plates and allowed to attach for 24 h.

Cells were assigned to eight experimental arms based on the applied treatments: Control (CON), CORT, CORT + DFO, CORT + Ferrostatin-1, Erastin, Erastin + GP, CORT + GP, and GP. The CON group was maintained in complete medium with no further intervention. The CORT group was stimulated with 400 μM CORT (≥ 98%, Yuanye Bio-Technology Co., Ltd., Shanghai, China) in complete medium for 24 h. The CORT + DFO and CORT + Ferrostatin-1 groups received a 30-min pre-exposure to either 100 μM DFO (Sigma-Aldrich, St. Louis, MO, USA) or 10 μM Ferrostatin-1 (Sigma-Aldrich, St. Louis, MO, USA) in complete medium, followed by a 24-h challenge with 400 μM CORT. The Erastin group was treated with 20 μM Erastin (Selleck. cn, Shanghai, China) in complete medium for 24 h. For the Erastin + GP group, a 30-min pre-incubation with 150 μg/mL GPs (≥ 98%, DeSiTe Bio-Technology Co., Ltd., Chengdu, China) was carried out before 24-h co-treatment with 20 μM Erastin. In the CORT + GP group, cells were pre-incubated with 150 μg/mL GPs for 30 min and subsequently co-stimulated with 400 μM CORT for 24 h. The GP group was incubated with 150 μg/mL GPs in complete medium alone for 24 h. The applied concentrations of Erastin [28], Ferrostatin-1 [29], and DFO [30] were adopted from earlier reports. Both CORT and GPs were solubilized in DMSO, ensuring the final DMSO level did not surpass 0.1%.

Cell viability assay

PC12 cells were plated at 5 × 10^3 cells per well in 100 μL of growth medium into 96-well plates. Following a 24-h attachment period, the cells were exposed to graded concentrations of CORT (0, 100, 200, 400, 800, and 1000 μM) and GPs (0, 50, 100, 150, and 200 μg/mL) for an additional 24 h. Cell viability was determined using the Cell Counting Kit-8 (Beyotime, Shanghai, China) according to the manufacturer's protocol.

ELISA kits assay

The amounts of IL-6, IL-1β, and TNF-α secreted into the culture medium of PC12 cells were measured using target-specific ELISA kits (Boster Biological Technology Co., Ltd., Wuhan, China) according to the manufacturer's instructions. Determination of ROS fluorescence intensity, MDA levels, and Glu and GSH concentrations in PC12 cells was performed using dedicated assay kits (Nanjing Jiancheng Bioengineering Institute, Nanjing, China) according to the provided protocols.

Iron accumulation assay

FerroOrange was used to visualize ferrous iron deposition in PC12 cells, with all steps performed as directed by the manufacturer (Dojido, Kumamoto, Japan). Fluorescent micrographs of cells co-labeled with FerroOrange and Hoechst were taken on a confocal fluorescence microscope (Leica, Wetzlar, Germany) at 400× magnification. Six unique, non-repeating fields were captured per group for quantitative analysis. Fluorescence intensities were processed using ImageJ 1.45.

LPO fluorescence intensity assay

Liperfluo was employed to assess LPO fluorescence intensity within PC12 cells, strictly following the manufacturer's instructions (Dojido, Kumamoto, Japan). Fluorescent images of cells co-stained with Liperfluo and Hoechst were obtained using a fluorescence microscope (Leica, Wetzlar, Germany) at 400× magnification. Six distinct, non-overlapping fields per group were recorded for statistical evaluation. Fluorescence intensity values were analyzed using ImageJ 1.45.

Western blot analysis

Protein isolation and Western blotting were executed as previously detailed [11, 31]. The primary antibodies applied included: anti-Hepcidin, anti-DMT1, anti-FPN1, anti-Ferritin, anti-GLS2, anti-SLC7A11, anti-GPX4, anti-TNFR1, anti-NF-κB, anti-p-NF-κB, anti-p53, anti-p-p53 (Abcam, Cambridge, UK), and anti-β-actin (ZSGE-BIO, Beijing, China).

Quantitative real-time PCR analysis

Total RNA was isolated from PC12 cells and reverse-transcribed to complementary DNA with the GoScript Reverse Transcription Kit (Promega Corporation, Madison, WI, USA). Quantitative real-time PCR was performed on a Roche 480 Real-Time PCR System (Roche, CH) using IQ SYBR Green Supermix (Bio-Rad, San Diego, CA, USA). Glyceraldehyde-3-phosphate dehydrogenase (GAPDH) served as the internal normalization control. Primer sequence information is compiled in **Table 1**. Full experimental procedures were outlined in our previous publication [11, 20].

Table 1. Primer sequence and amplification length of the destination fragment.

Gene	Number	Upstream and downstream primer sequence	Product length (bp)
Hepcidin	NM_053469.2	F: CTATCTCCGGCAACAGACGA R: TGTCTCGCTTCCTTCGCTTC	110
DMT1	NM_013173.2	F: TGGTTAGCGTGGCTTATCTGG R: AGTATTGCCACCGCTGGTATC	143
FPN1	NM_133315.2	F: TGGGAGCATCAGCAATAAC R: CAGACCAGTCCGAACAAGG	86
Ferritin	NM_022500.5	F: GGAACTTCACAAACTGGCTAC R: TGGATTTCACCTGCTCATT	89
GLS2	NM_001270786.1	F: GGGTGTCCGGTACTACTTCG R: GTTCGAGGCATCATGGTCCG	94
GPX4	NM_001039849.3	F: GACCTTCCCCAGACCAGCAAC R: CGCAACCCCTGTACTTATCCAG	145
SLC7A11	NM_001107673.3	F: TCAAATCCTTGGCCATCTGC R: ACCAATTCCTTTAGCCCATCATC	92
IL-6	NM_012589.2	F: CTTCTTGGGACTGATGTTG R: TACTGGTCTGTTGTGGGTG	97
IL-1β	NM_031512.2	F: CTCGTGGGATGATGACGACC R: AGCTTTCAGCTCACATGGGT	118
TNF-α	NM_012675.3	F: GCCACCACGCTCTTCTGTC R: GCTACGGGCTTGTCACTCG	149
TNFR1	NM_013091.2	F: CCAAGTGCCACAAAGGAACC R: GTGCCTTTATCACACACCTCG	85
NF-κB	NM_199267.2	F: ACTGCCGGGATGGCTTCTAT R: CTTGCTCCAGGTCTCGCTTC	105
p53	NM_030989.3	F: AGCGACTACAGTTAGGGGGT R: ACAGTTATCCAGTCTTCAGGGG	89
GAPDH	NM_017008.4	F: GGCAAGTTCAACGGCACAG R: CGCCAGTAGACTCCACGAC	142

Statistical analysis

Data were reported as mean ± standard deviation (SD) and handled with SPSS software (version 22.0; SPSS, Chicago, IL, USA). Student's t-test was employed for pairwise comparisons, whereas analysis of variance (ANOVA) with Tukey's post hoc correction was applied for comparisons spanning multiple groups. Every experiment included six biological replicates, each with three technical replicates. A threshold of $P < 0.05$ was adopted to indicate statistical significance.

Results and Discussion

Effects of DFO and ferrostatin-1 on CORT-induced PC12 cells viability

The dose-dependent cytotoxicity of CORT toward PC12 cells is depicted in **Figure 1a**. The half-maximal inhibitory concentration (IC50) of CORT in PC12 cells was determined to be 458 μM using GraphPad Prism 10.1.2. We reviewed published reports on the working concentration window of CORT and observed that the range used to generate the CORT-induced PC12 cell injury paradigm mostly spanned 100 μM to 800 μM. On this basis, 400 μM CORT (approximating the IC50) was picked for all subsequent experimentation. Under this regimen, the fraction of surviving PC12 cells declined sharply.

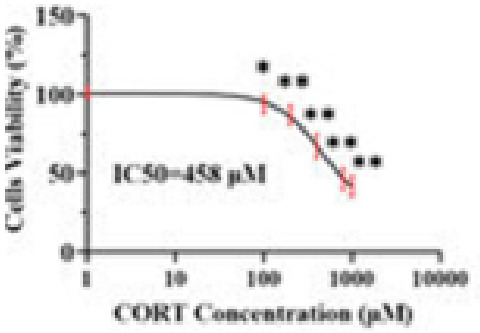

a)

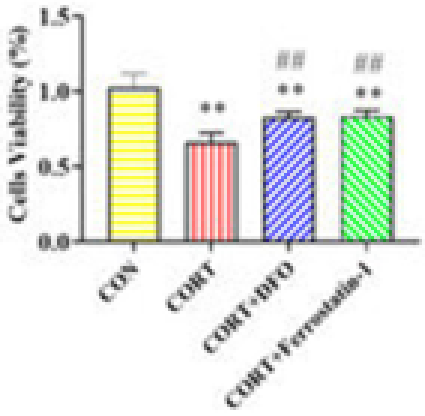

b)

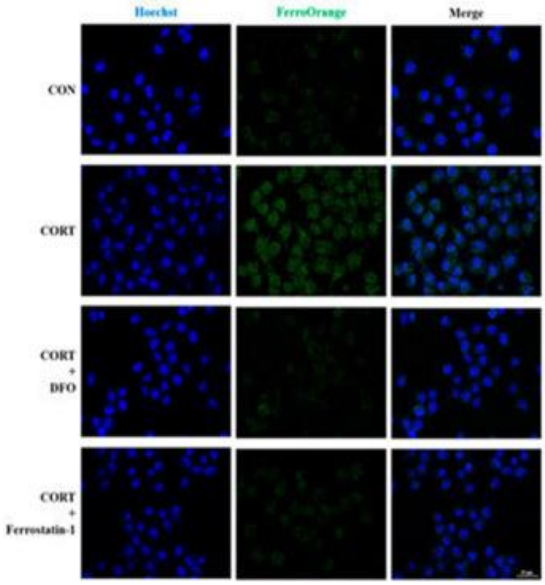

c)

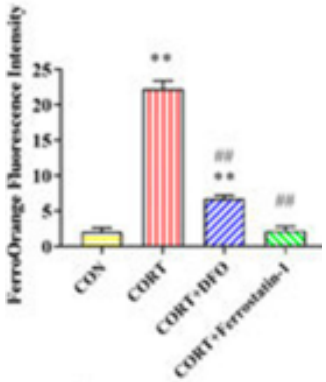

d)

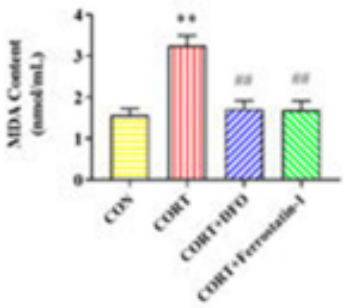

e)

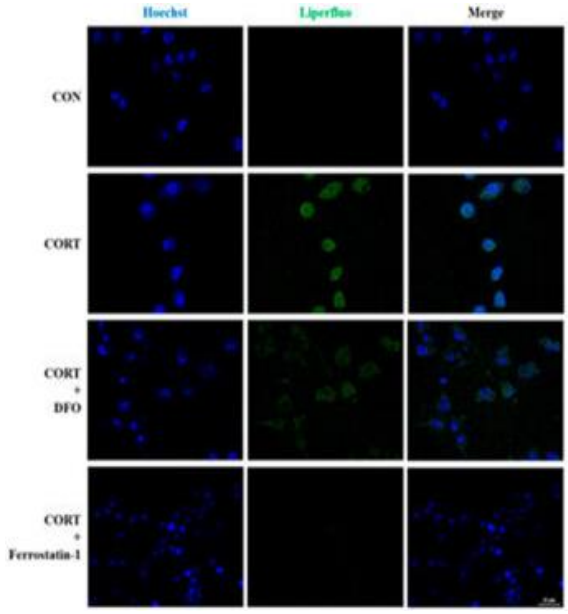

f)

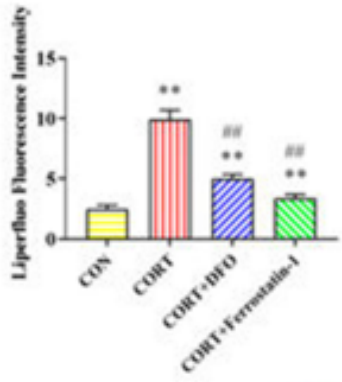

g)

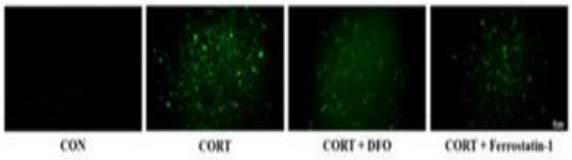

h)

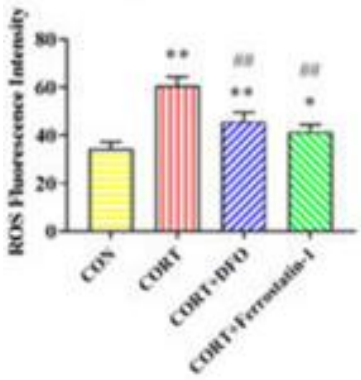

i)

Figure 1. Effects of DFO and Ferrostatin-1 on CORT-induced ferroptosis in PC12 cells: (a) Viability of PC12 cells following exposure to varying CORT concentrations. (b) PC12 cell viability under different treatment conditions. (c) Representative immunofluorescence images of FerroOrange (green)

positive cells captured at 400× magnification. Nuclei were counterstained with Hoechst (blue) in PC12 cells. Scale bar = 25 μm. (d) Iron fluorescence intensity. (e) MDA content. (f) Representative immunofluorescence images of Liperfluo (green) positive cells obtained at 400× magnification. Nuclei were counterstained with Hoechst (blue) in PC12 cells. Scale bar = 25 μm. (g) LPO fluorescence intensity. (h) Representative ROS immunofluorescence images of PC12 cells viewed at 200× magnification. Scale bar = 50 μm. (i) ROS fluorescence intensity. All data are expressed as the mean ± SD (n = 6). $P < 0.05$ and $P < 0.01$ compared with the CON group. ## $P < 0.01$ compared with the CORT group.

The influence of the various pharmacological treatments on PC12 cell viability is shown in **Figure 1b**. Relative to the CON group, cell viability was reduced in the CORT group. When compared with the CORT group, cell viability was markedly elevated in the CORT + DFO and CORT + Ferrostatin-1 groups. These findings demonstrate that DFO and Ferrostatin-1 enhance the survival of CORT-challenged PC12 cells.

Effect of DFO and ferrostatin-1 on CORT-induced PC12 cells iron accumulation

The immunofluorescent staining data for iron in PC12 cells are displayed in **Figures 1c and 1d**. When compared with the CON group, the FerroOrange (green) fluorescent signal in PC12 cells was substantially increased in the CORT group. In contrast, it was appreciably lowered in the CORT + DFO and CORT + Ferrostatin-1 groups compared with the CORT group. These results indicate that DFO and Ferrostatin-1 can relieve iron overload induced by CORT in PC12 cells.

Effect of DFO and ferrostatin-1 on CORT-induced lipid peroxidation in PC12 cells

Figures 1e–1i portray the assay results for lipid peroxidation-associated parameters in PC12 cells. In contrast to the CON group, MDA levels, along with the fluorescent signals of Liperfluo and ROS, showed a clear increase in the CORT group. Conversely, these lipid peroxidation markers were meaningfully reduced in the CORT + DFO and CORT + Ferrostatin-1 groups relative to the CORT group. These outcomes imply that CORT exposure can induce lipid peroxidation and that DFO, along with Ferrostatin-1, reduces lipid peroxide accumulation in PC12 cells.

Effect of GPs on erastin-induced viability of PC12 cells

Within the Erastin group, PC12 cells viability fell considerably below that of the CON group, whereas in the Erastin + GP group, it rose substantially above the Erastin group value **(Figure 2a)**. These data indicate that GPs enhance cell survival in PC12 cells subjected to an Erastin challenge.

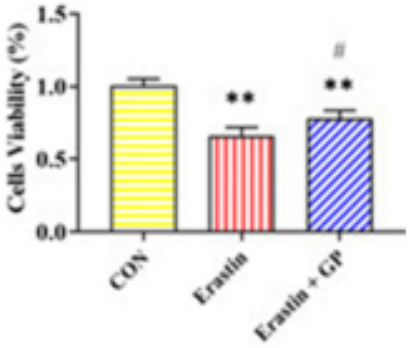

a)

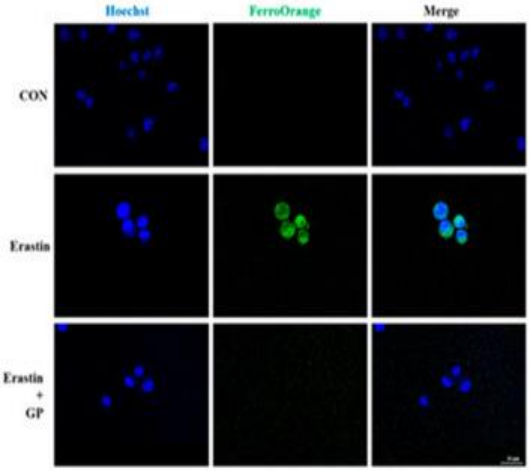

b)

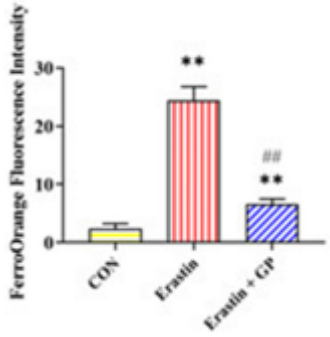

c)

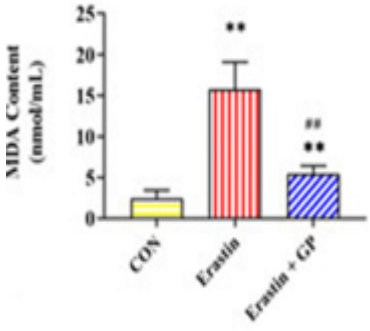

d)

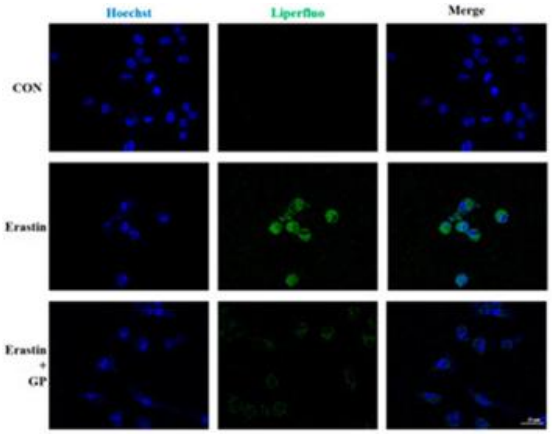

e)

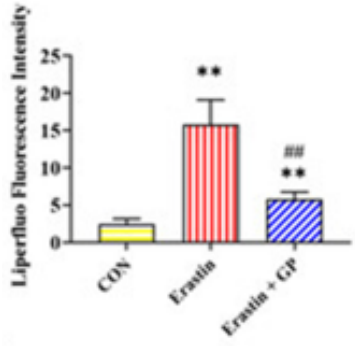

f)

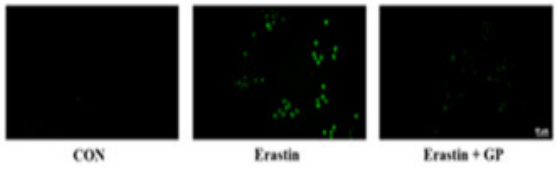

g)

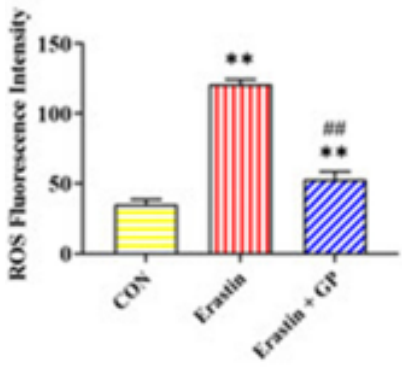

h)

Figure 2. Effects of GPs on Erastin-induced ferroptosis in PC12 cells: (a) Survival of PC12 cells across distinct treatment conditions. (b) Representative immunofluorescence micrographs of FerroOrange (green) positive cells acquired at 400× magnification. Nuclei were labeled with Hoechst (blue) in PC12 cells. Scale bar = 25 μm. (c) Quantified iron fluorescence intensity. (d) Measured MDA levels. (e) Representative immunofluorescence micrographs of Liperfluo (green) positive cells obtained at 400× magnification. Nuclei were labeled with Hoechst (blue) in PC12 cells. Scale bar = 25 μm. (f) Quantified LPO fluorescence intensity. (g) Representative immunofluorescence micrographs depicting ROS in PC12 cells imaged at 200× magnification. Scale bar = 50 μm. (h) Quantified ROS fluorescence intensity. All data are expressed as the mean ± SD (n = 6). $P < 0.01$ compared against the CON group. # $P < 0.05$ and ## $P < 0.01$ compared against the CORT group.

Effect of GPs on erastin-induced iron accumulation in PC12 cells

The immunofluorescent staining outcomes for iron in PC12 cells are presented in **Figures 2b and 2c**. When set against the CON group, the FerroOrange fluorescent signal underwent a sizable elevation in the Erastin group within PC12 cells. Compared with the Erastin group, the FerroOrange fluorescent signal dropped substantially in the Erastin + GP group. These data imply that GPs can attenuate the iron overload provoked by Erastin in PC12 cells.

Effect of GPs on erastin-induced lipid peroxidation in PC12 cells

Figures 2d–2h shows the assay results for lipid peroxidation-linked indicators in PC12 cells. MDA content, together with Liperfluo and ROS fluorescence intensities, climbed steeply in the Erastin group relative to the CON group. In contrast, these measures declined more notably in the Erastin + GP group than in the Erastin group. These results establish that GPs can counteract Erastin-driven lipid peroxidation in PC12 cells.

Effect of GPs on CORT-induced PC12 cells viability

Figures 3a and 3b portray the effect of GPs on the viability of PC12 cells challenged with CORT. Application of 400 μM CORT resulted in a pronounced decrease in the survival rate of PC12 cells. However, the introduction of 100, 150, and 200 mg/mL GPs resulted in a marked increase in the survival rate of PC12 cells. Notably, 150 mg/mL GPs conferred the most favorable protective effect without obvious harm to cells, and doses exceeding this threshold did not meaningfully enhance it. These observations indicate that GPs elevate the viability of CORT-stressed PC12 cells. As a result, 150 mg/mL GPs was adopted for all subsequent cellular investigations.

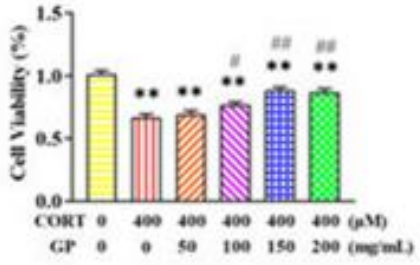
Cell Viability (%)
1.5
1.0
0.5
0.0
CORT 0 400 400 400 400 400 (μM)
GP 0 0 50 100 150 200 (ng/mL)

a)

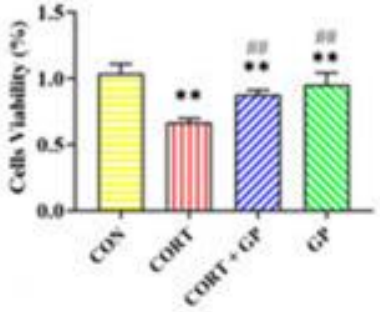
Cells Viability (%)
1.5
1.0
0.5
0.0
CON
CORT
CORT + GP
GP

b)

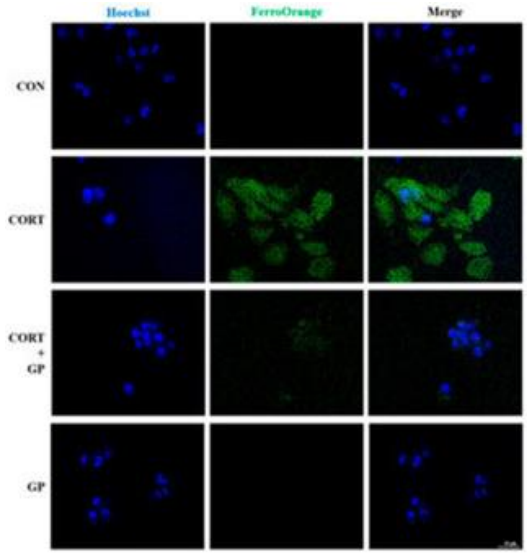
Hoechst
FerroOrange
Merge
CON
CORT
CORT + GP
GP

c)

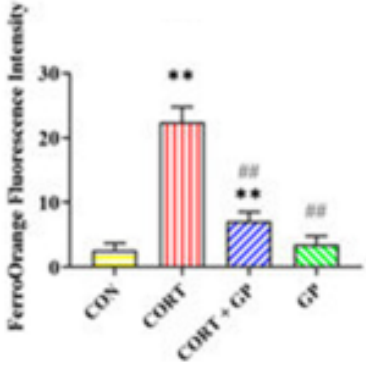
FerroOrange Fluorescence Intensity
30
20
10
0
CON
CORT
CORT + GP
GP

d)

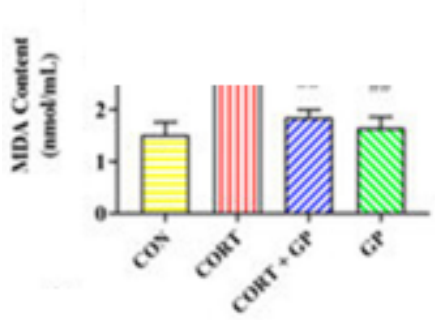
MDA Content (nmol/mL)
2
1
0
CON
CORT
CORT + GP
GP

e)

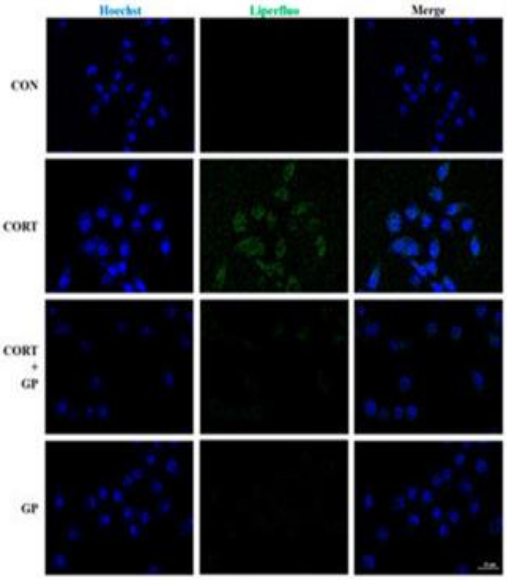
Hoechst
Liperfluo
Merge
CON
CORT
CORT + GP
GP

f)

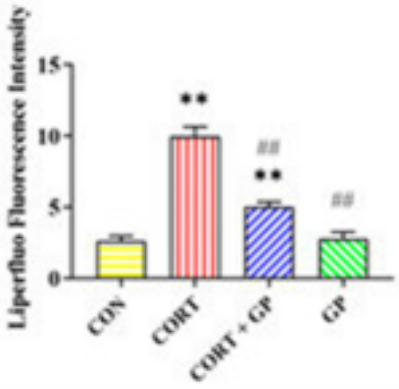
Liperfluo Fluorescence Intensity
15
10
5
0
CON
CORT
CORT + GP
GP

g)

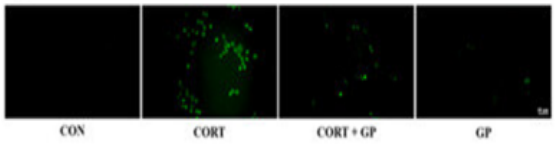
CON
CORT
CORT + GP
GP

h)

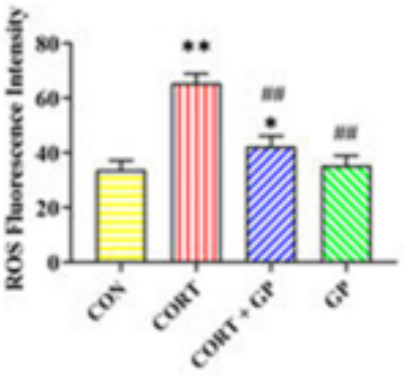

i)

Figure 3. Effects of GPs on CORT-induced ferroptosis in PC12 cells: (a) Impact of various GP concentrations on the survival of PC12 cells treated with 400 μM CORT. (b) Cell survival rates in the different treatment arms. (c) Representative immunofluorescence micrographs of FerroOrange (green) positive cells acquired at 400× magnification. Nuclei were labeled with Hoechst (blue) in PC12 cells. Scale bar = 25 μm. (d) Quantified iron fluorescence intensity. (e) Measured MDA levels. (f) Representative immunofluorescence micrographs of Liperfluo (green) positive cells obtained at 400× magnification. Nuclei were labeled with Hoechst (blue) in PC12 cells. Scale bar = 25 μm. (g) Quantified LPO fluorescence intensity. (h) Representative immunofluorescence micrographs depicting ROS in PC12 cells imaged at 200× magnification. Scale bar = 50 μm. (i) Quantified ROS fluorescence intensity. All data are expressed as the mean ± SD (n = 6). $P < 0.05$ and $P < 0.01$ compared against the CON group. # $P < 0.05$ and ## $P < 0.01$ compared against the CORT group.

Effect of GPs on CORT-induced PC12 cells iron accumulation

The immunofluorescent staining data for iron in PC12 cells are shown in **Figures 3c and 3d**. Compared with the CON group, the FerroOrange fluorescent signal increased sharply in the CORT group. Compared with the CORT group, the FerroOrange fluorescent signal decreased substantially in the CORT + GP group. These observations imply that GP can alleviate iron overload induced by CORT in PC12 cells.

Effect of GPs on CORT-induced PC12 cells lipid peroxidation

Figures 3e–3i portray the assay results for lipid peroxidation-linked indicators in PC12 cells. MDA levels, along with Liperfluo and ROS fluorescent intensities, were substantially higher in the CORT group than in the CON group. At the same time, those same measures were markedly lower in the CORT + GP group than in the CORT group. These data indicate that GPs can counteract CORT-driven lipid peroxidation in PC12 cells.

Effect of GPs on CORT-induced PC12 cells iron homeostasis

The mRNA and protein expression patterns of iron homeostasis-associated proteins in PC12 cells are depicted in **Figure 4**. Compared with the CON group, the mRNA and protein expression of Hepcidin and DMT1 increased, whereas those of FPN1 and Ferritin decreased in the CORT group. Compared with the CORT group, mRNA and protein expression of Hepcidin and DMT1 were considerably diminished. In contrast, the mRNA and protein expression of FPN1 and Ferritin were considerably augmented in the CORT + GP group. These results establish that GPs restore the imbalance in iron homeostasis induced by CORT in PC12 cells.

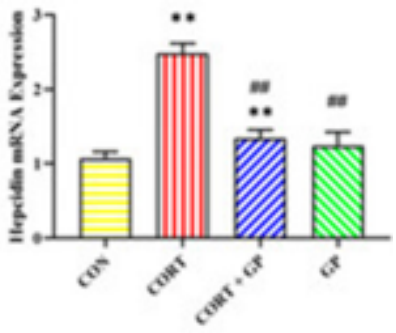

a)

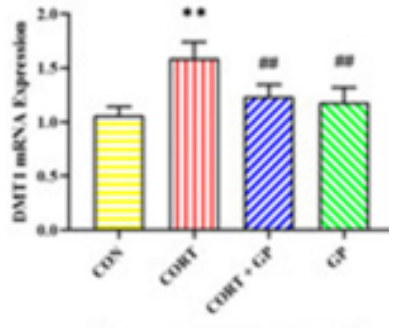

b)

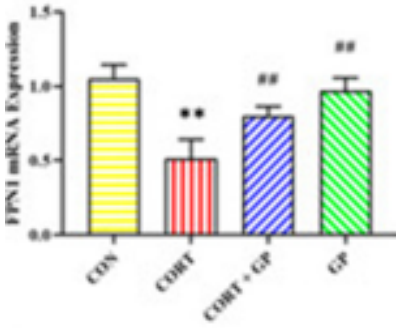

c)

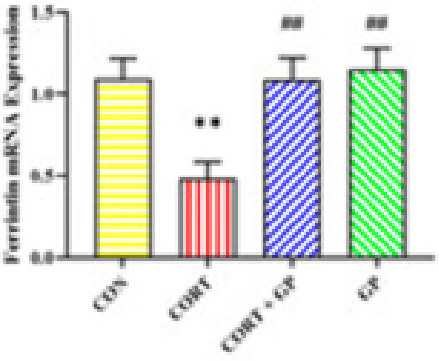

d)

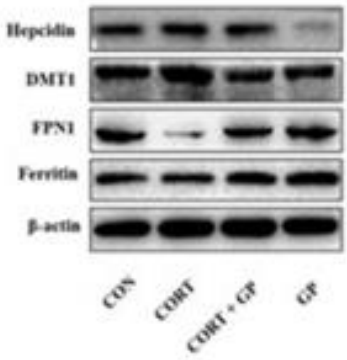

e)

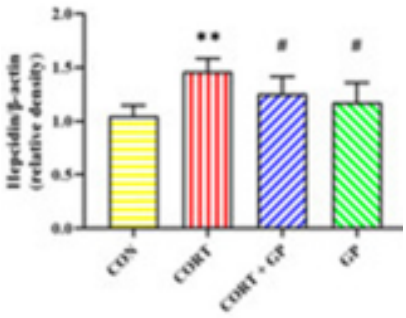

f)

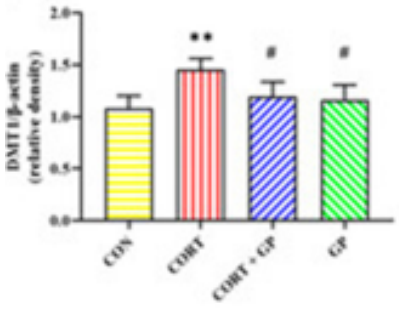

g)

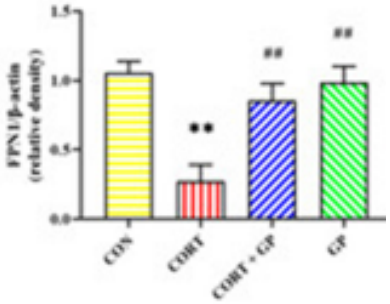

h)

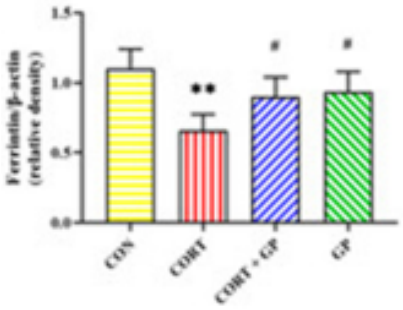

i)

Figure 4. Effects of GPs on CORT-induced iron metabolism in PC12 cells: (A–D) Quantification of relative mRNA levels for Hepcidin, DMT1, FPN1, and Ferritin. (E) Representative protein bands for Hepcidin, DMT1, FPN1, and Ferritin. (F–I) Densitometric quantification of Hepcidin, DMT1, FPN1, and Ferritin protein expression. All data are expressed as the mean ± SD (n = 6). $P < 0.01$ compared with the CON group. # $P < 0.05$ and ## $P < 0.01$ compared with the CORT group.

Effect of GPs on CORT-induced PC12 cells glu metabolism

The measured concentrations of Glu and GSH within PC12 cells are presented in **Figures 5a and 5b**. When compared with the CON group, Glu levels increased steeply in the CORT group, and a pronounced reduction was observed in the CORT + GP group relative to the CORT group. Compared with the CON group, GSH levels dropped sharply in the CORT group. On the other hand, GSH levels rebounded considerably in the CORT + GP group versus the CORT group.

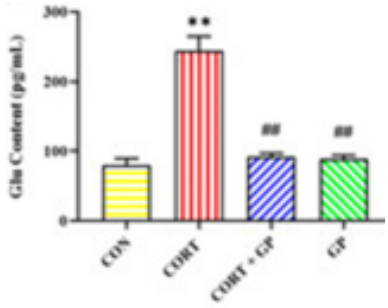

a)

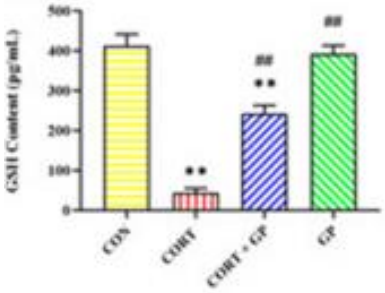

b)

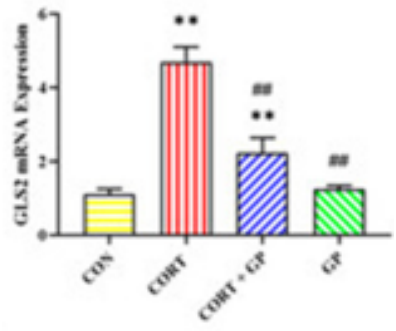

c)

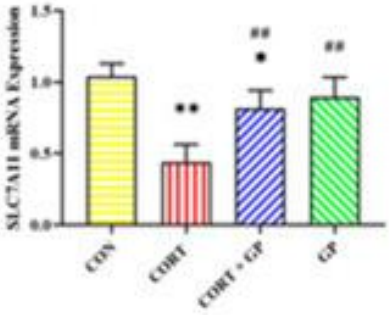

d)

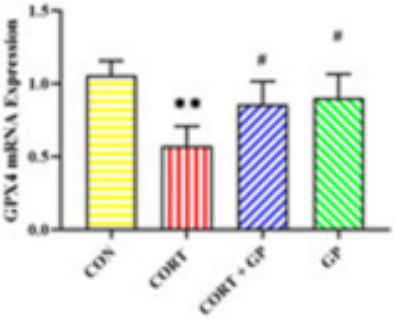

e)

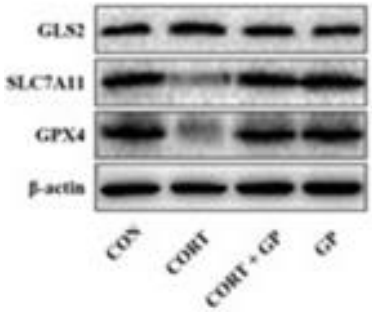

f)

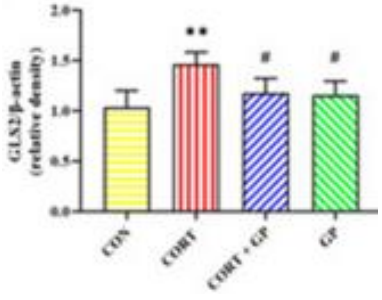

g)

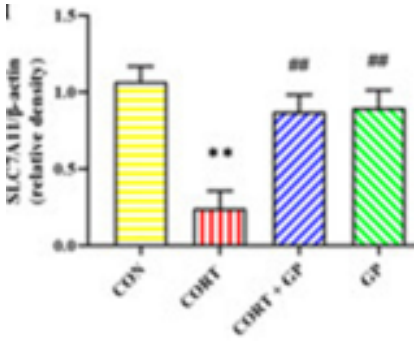

h)

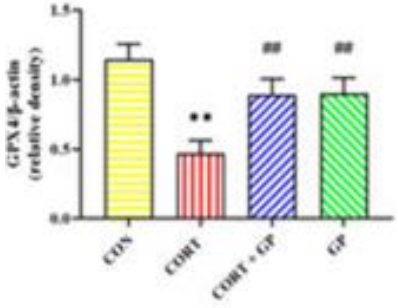

i)

Figure 5. Effects of GPs on the CORT-induced Glu metabolism in PC12 cells: (a, b) Glu and GSH concentrations. (c–e) Relative mRNA expression levels of GLS2, SLC7A11, and GPX4. (f) Representative protein bands for GLS2, SLC7A11, and GPX4. (g–i) Densitometric analysis of GLS2, SLC7A11, and GPX4 protein expression. All data are expressed as the mean ± SD (n = 6). $P < 0.05$ and $P < 0.01$ compared with the CON group. # $P < 0.05$ and ## $P < 0.01$ compared with the CORT group.

The mRNA and protein expression patterns of Glu metabolism-associated proteins in PC12 cells are displayed in **Figures 5c–5i**. When set against the CON group, the mRNA and protein levels of GLS2 rose sharply, while those of SLC7A11 and GPX4 fell sharply in the CORT group. Contrasted with the CORT group, the mRNA and protein levels of GLS2 dropped significantly, whereas those of SLC7A11 and GPX4 climbed significantly in the CORT + GP group. These data confirm that GPs can notably rectify the Glu metabolic disturbances triggered by CORT in PC12 cells.

Effect of GPs on CORT-induced release of inflammatory cytokines in PC12 cells

The measured concentrations, along with the mRNA expression data for inflammatory cytokines, are shown in **Figure 6**. The amounts and mRNA expression of IL-6, IL-1β, and TNF-α recorded in the CORT group exceeded those in the CON group by a considerable margin. In contrast, in the CORT + GP group, these same inflammatory factors were substantially reduced compared to the CORT group. These observations indicate

that GPs can restrain the outpouring of inflammatory cytokines instigated by CORT in PC12 cells.

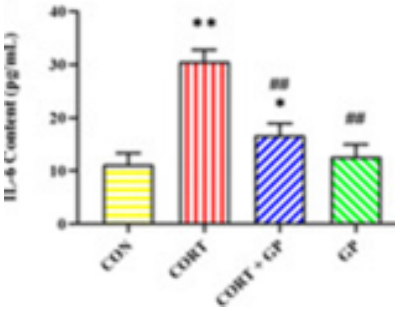

a)

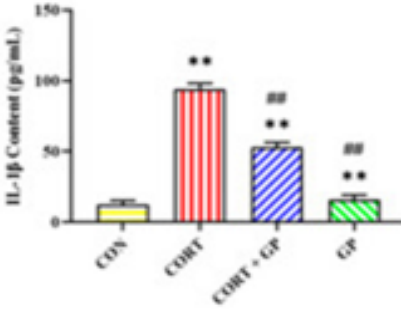

b)

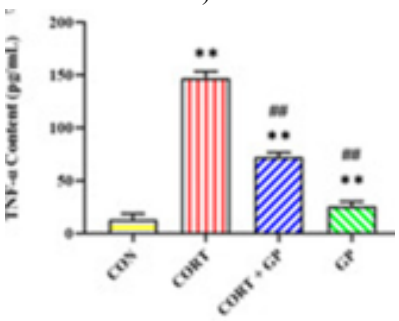

c)

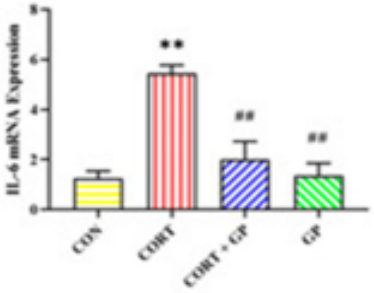

d)

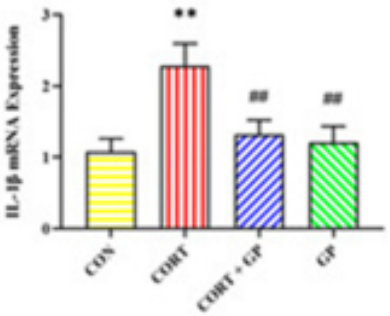

e)

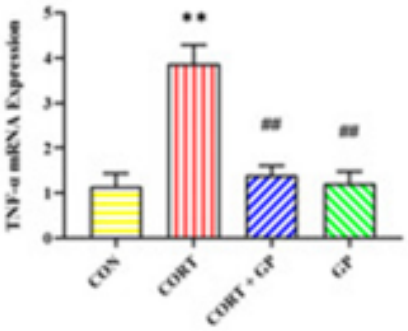

f)

Figure 6. Effect of GPs on the CORT-induced release of inflammatory cytokines in PC12 cells. (a–c) Concentrations of IL-6, IL-1β, and TNF-α were measured in the culture supernatant. (d–f) Relative mRNA expression levels of IL-6, IL-1β, and TNF-α in PC12 cells. All data are expressed as the mean ± SD (n = 6). $P < 0.05$ and $P < 0.01$ compared with the CON group. ## $P < 0.01$ compared with the CORT group.

Effect of GPs on CORT-induced TNF-α/NF-κB signaling pathway in PC12 cells

The mRNA expression of TNFR1, NF-κB, and p53 underwent a significant upsurge in the CORT group relative to the CON group. In contrast, these transcripts were substantially lessened in the CORT + GP group compared with the CORT group **(Figures 7a–7c)**. In a parallel fashion, the protein abundance of TNFR1, p-NF-κB, NF-κB, p-p53, and p53 in the CORT group was noticeably heightened compared with the CON group. Still, these protein levels dropped appreciably in the CORT + GP group in contrast to the CORT group **(Figures 7d–7i)**. Moreover, the ratios of p-NF-κB to total NF-κB and of p-p53 to total p53 increased substantially in the CORT group compared with the CON group. Yet, these same ratios decreased markedly in the CORT + GP group compared with the CORT group **(Figures 7j and 7 k)**. These data imply that GPs restrain the activation of the TNF-α/NF-κB signaling axis triggered by CORT in PC12 cells.

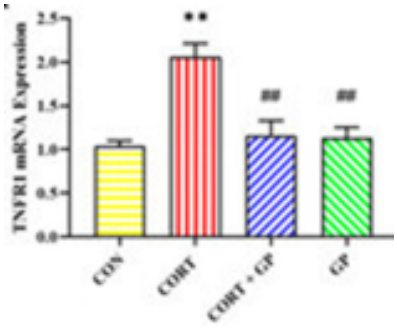

a)

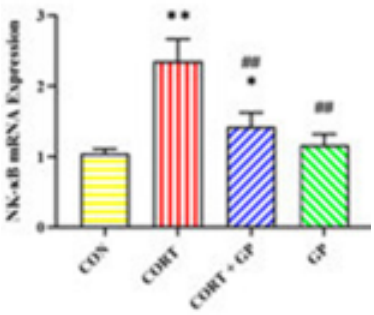

b)

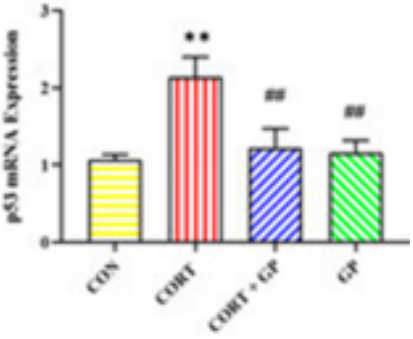

c)

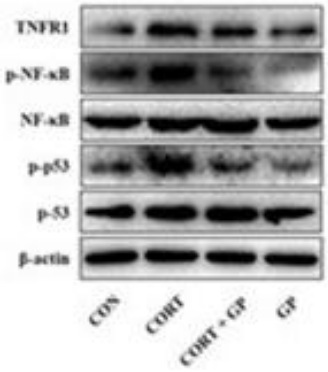

d)

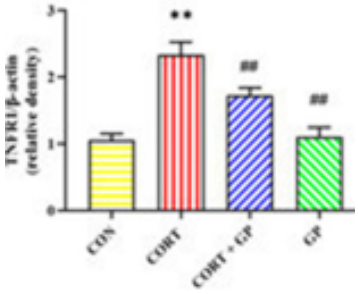

e)

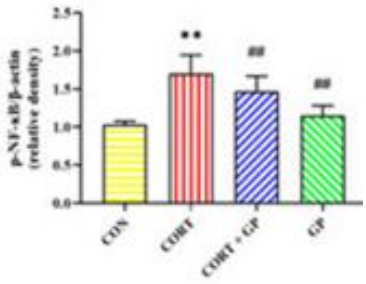

f)

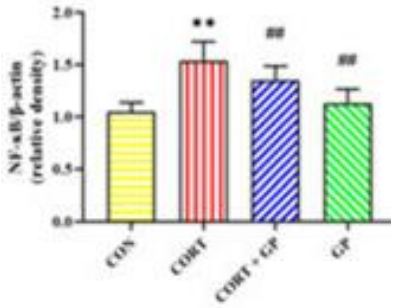

g)

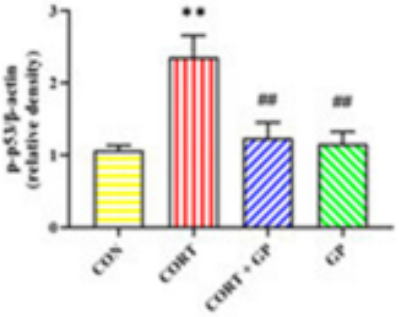

h)

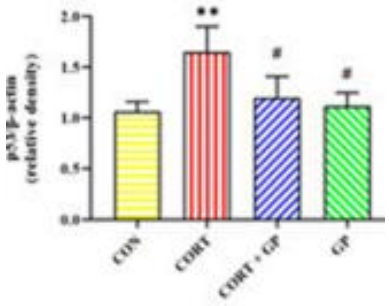

i)

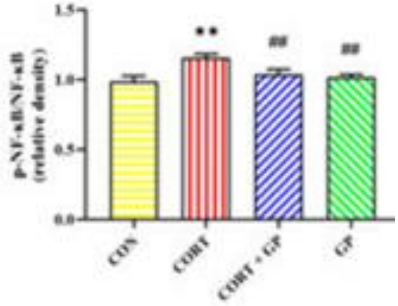

j)

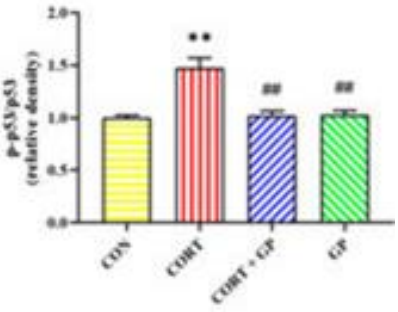

k)

Figure 7. Effect of GPs on CORT-induced TNF-α/NF-κB signaling pathway in PC12 cells: (a–c) Relative mRNA expression levels of TNFR1, NF-κB, and p53.

(d) Representative protein bands of TNFR1, p-NF-κB, NF-κB, p-p53, and p53. (e–i) Densitometric quantification of TNFR1, p-NF-κB, NF-κB, p-p53, and p53 protein expression. (J) Ratio of p-NF-κB to NF-κB protein expression. (k) Ratio of p-p53 to p53 protein expression. All data are expressed as the mean ± SD (n = 6). $P < 0.05$ and $P < 0.01$ compared with the CON group. # $P < 0.05$ and ## $P < 0.01$ compared with the CORT group.

Sustained stress can provoke neural harm in animals, culminating in neuroimmune dysregulation and atypical behavioral patterns [1, 15]. Our prior investigations revealed that blocking ferroptosis relieved hippocampal injury and depressive-like manifestations stemming from persistent stress [7, 11]. Still, low-cost, potent feed additives or therapeutic formulations to tackle chronic stress-linked neurological disorders in the livestock industry await further discovery. In the current work, we demonstrated that GPs could suppress ferroptosis in neural cells triggered by chronic stress in vitro, using selective ferroptosis inhibitors and inducers. Additionally, GPs mitigated CORT-driven ferroptosis in neural cells by downregulating TNF-α/NF-κB signaling.

GPs possess robust anti-inflammatory and antioxidant properties. Regarding the selection of GPs concentration and treatment duration, we reviewed existing publications. We noted that GPs at 25–800 μg/mL were effective in attenuating hydrogen peroxide-induced damage to rat retinal ganglion cells [16]. Separately, 200 μg/mL GP can counteract Glu-induced injury in primary cortical cells [32]. In our hands, 150 mg/mL GPs yielded the optimal protective effect while causing no discernible harm to the cells.

Ferroptosis is a newly recognized type of programmed cell death characterized by the accumulation of lipid peroxides and ROS, along with prominent intracellular iron deposition [5]. Since surplus LPO drives ferroptosis, LPO constitutes a key indicator of this form of cell death [5]. MDA is a breakdown product of membrane lipid peroxidation and can serve as an indirect gauge of cellular lipid oxidative damage. FerroOrange and Liperfluo, which act as fluorescent sensors for ferrous ions and LPO, respectively, are routinely used for ferroptosis detection [33]. To further interrogate whether the neuronal impairment induced by CORT is connected to ferroptosis, CORT-stimulated PC12 cells were pretreated with DFO and Ferrostatin-1 in this experimental setup. We demonstrated that CORT provoked iron overload and lipid peroxidation in PC12 cells, whereas DFO and Ferrostatin-1 overturned both phenomena. These data suggest that CORT can elicit ferroptosis in PC12 cells.

Erastin is commonly deployed as a ferroptosis agonist [6]. Meanwhile, GPs exhibit neuroprotective effects and improve cognitive deficits. To clarify whether the neuroprotective effect of GPs was linked to ferroptosis, this investigation pretreated Erastin-challenged PC12 cells with GPs. We confirmed that GPs could alleviate ferroptosis in PC12 cells by mitigating Erastin-induced oxidative stress, lipid peroxidation, cellular iron accumulation, and cell lethality.

To examine the protective role of GPs against CORT-induced ferroptosis in PC12 cells, we applied GP pretreatment to CORT-exposed PC12 cells. The data showed that GPs reversed CORT-elicited ferroptosis in PC12 cells. Consistently, GPs have been documented to ease neuronal damage produced by hydrogen peroxide [16] and by chronic unpredictable mild stress [18]. Collectively, these lines of evidence establish that the neuroprotection conferred by GPs is intimately tied to the suppression of ferroptosis.

Iron homeostasis in neurons is rigorously maintained by iron-regulatory proteins, namely Hepcidin, DMT1, FPN1, and Ferritin [9]. Hepcidin, a pivotal downstream effector governing iron distribution among different iron reservoirs, can negatively modulate DMT1 and FPN1 levels in response to triggers such as injury, infection, and inflammation, thus serving as a rheostat of iron balance [12]. DMT1 is responsible for iron import, while FPN1 provides the sole conduit for iron export [9]. In addition, Ferritin levels display an inverse relationship with intracellular iron content. The degradation of ferritin increases free iron levels within cells and worsens neuronal damage [9]. Studies have reported that chronic mild stress can boost Hepcidin expression, consequently elevating DMT1 and diminishing FPN1 and ferritin, a sequence that leads to iron deposition in the hippocampus [12]. Furthermore, CORT evokes disordered iron metabolism in cultured hippocampal neurons [26]. In the present study, GPs could alleviate CORT-triggered imbalance in iron homeostasis by correcting the expression of key iron metabolism proteins in PC12 cells.

Beyond that, Glu metabolism constitutes another regulatory axis for ferroptosis [9]. Glu is produced through the hydrolysis of glutamine by glutaminase and can undergo pronounced accumulation under pathological circumstances [5]. Under normal physiology, the System Xc^- (cystine/Glu antiporter) mediates the exchange of cystine and Glu at a 1:1 stoichiometry, with SLC7A11 representing a light-chain component of this transporter [5]. GSH is primarily derived from cystine and functions as a vital intracellular antioxidant. Nevertheless, elevated Glu concentrations compromise the activity of System Xc^-, thereby constraining GSH biosynthesis. Impaired GSH synthesis can dismantle the antioxidant defense, permitting massive accumulation of LPO and lipid ROS, an event that culminates in neuronal ferroptosis [5]. In parallel, GPX4 acts as a negative regulator of lipid peroxidation by converting potentially toxic lipid

hydroperoxides into innocuous lipid alcohols at the expense of GSH. The abrogation of GSH production inactivates GPX4, triggering extensive LPO buildup and ultimately neuronal ferroptosis [8]. Therefore, GSH depletion and GPX4 inactivation likewise represent defining traits of ferroptosis. In the current study, GPs could ameliorate CORT-evoked neuronal ferroptosis by restoring proper Glu metabolism in PC12 cells.

We measured the secretion of inflammatory cytokines in this investigation to further probe the protective mechanism underlying GPs' effects on CORT-elicited neuronal ferroptosis. Our data revealed that GPs lowered both the release and expression of inflammatory cytokines in PC12 cells. Hence, the protective action of GPs against ferroptosis is intimately connected to the suppression of inflammatory cytokines and their associated signaling cascades. A growing body of evidence indicates that the TNF-α/NF-κB signaling pathway can directly govern the expression of several pivotal genes and proteins implicated in ferroptosis, including p53 [20]. The p53 protein serves as a critical regulatory node in ferroptosis [24]. It can not only upregulate GLS2 gene expression to promote Glu production but also directly repress SLC7A11 expression, culminating in GSH exhaustion and consequent lipid peroxidation [25]. Our findings implied that GPs restrained the activation of the CORT-triggered TNF-α/NF-κB signaling axis in PC12 cells.

Furthermore, GPs reduced the phosphorylation of both NF-κB and p53. Consistent with this, GPs exert a neuroprotective effect by inhibiting the release of inflammatory cytokines and dampening NF-κB signaling in the hippocampus [18]. Taken together, the suppression of the TNF-α/NF-κB signaling pathway constitutes the core molecular mechanism through which GPs mitigate CORT-induced ferroptosis in PC12 cells.

Nevertheless, the present study carries certain limitations. The principal constituents of GPs encompass Gypenoside L, Gypenoside LI, and Gypenoside XLIX, among others. The GP preparation used here was analyzed by high-performance liquid chromatography, which identified Gypenoside XLIX as the predominant component, along with Rutin, Isorhamnetin, Quercetin, Allose, Linoleic acid, and others. All of the aforementioned are constituents of the Gypenoside extract; however, the effects of the Gypenoside XLIX monomer remain to be explored in future studies. In addition, the neuroprotective mechanism of GPs likely involves multiple signaling pathways across different pathological models [34]. Currently, corresponding pathway validation and animal regression experiments are lacking. Our research group is undertaking the next phase of experimentation to address this gap. In the future, linking the research outcomes to the development of potential therapeutic agents should be a priority.

Conclusion

The present study uncovered a novel neuroprotective mechanism by which GPs attenuate neuronal ferroptosis triggered by chronic stress. In particular, GPs alleviated CORT-induced ferroptosis in PC12 cells through inhibiting the TNF-α/NF-κB signaling pathway, diminishing the secretion of inflammatory mediators, rectifying iron metabolic disturbance and iron overload, and suppressing p53 phosphorylation to ameliorate glutamate metabolism disruption and curtail lipid peroxide accumulation. This work offers fresh mechanistic insight into neuronal death caused by chronic stress. It provides experimental and theoretical foundations for the application of GPs in the prevention and management of chronic stress in animal husbandry.

Acknowledgments: This study was supported by the Department of Surgery and Obstetrics, College of Veterinary Medicine, South China Agricultural University.

Conflict of interest: None

Financial support: This study was supported by the National Natural Science Foundation of China (Grant No. 32102746), the special topic of basic and applied research in Guangzhou (Grant No. 2023A04J0758), the specific university discipline construction project in Guangdong Province (Grant No. 2023B10564003), and the Natural Science Foundation of Guangdong Province (Grant No. 2025A1515011619).

Ethics statement: None

References

1. Menneson S, Ménicot S, Ferret-Bernard S, Guérin S, Romé V, Le Normand L, et al. Validation of a psychosocial chronic stress model in the pig using a multidisciplinary approach at the gut-brain and behavior levels. Front Behav Neurosci. 2019;13:161.
2. Prims S, Vanden Hole C, Van Cruchten S, Van Ginneken C, Van Ostade X, Casteleyn C. Hair or salivary cortisol analysis to identify chronic stress in piglets? Vet J. 2019;252:105357.
3. Noushad S, Ahmed S, Ansari B, Mustafa UH, Saleem Y, Hazrat H. Physiological biomarkers of chronic stress: a systematic review. Int J Health Sci (Qassim). 2021;15(5):46-59.
4. Milligan Armstrong A, Porter T. Chronic stress and Alzheimer's disease: the interplay between the hypothalamic-pituitary-adrenal axis, genetics and microglia. Biol Rev Camb Philos Soc. 2021;96(5):2209-28.

5. Stockwell BR, Friedmann Angeli JP, Bayir H, Bush AI, Conrad M, Dixon SJ, et al. Ferroptosis: a regulated cell death nexus linking metabolism, redox biology, and disease. Cell. 2017;171(2):273-85.
6. Dixon SJ, Lemberg KM, Lamprecht MR, Skouta R, Zaitsev EM, Gleason CE, et al. Ferroptosis: an iron-dependent form of nonapoptotic cell death. Cell. 2012;149(5):1060-72.
7. Zhang H, Sun Q, Peng J, Zhao Y, Wei M, Fan H. Lycopene alleviates chronic stress-induced hippocampal microglia ferroptosis by inhibiting the ASK1/JNK signaling pathway. Food Biosci. 2025;64:105859.
8. Hambright WS, Fonseca RS, Chen L, Na R, Ran Q. Ablation of ferroptosis regulator glutathione peroxidase 4 in forebrain neurons promotes cognitive impairment and neurodegeneration. Redox Biol. 2017;12:8-17.
9. Masaldan S, Bush AI, Devos D, Rolland AS, Moreau C. Striking while the iron is hot: iron metabolism and ferroptosis in neurodegeneration. Free Radic Biol Med. 2019;133:221-33.
10. Mehrpouya S, Nahavandi A, Khojasteh F, Soleimani M, Ahmadi M, Barati M. Iron administration prevents BDNF decrease and depressive-like behavior following chronic stress. Brain Res. 2015;1596:79-87.
11. Zhang H, Jiao W, Cui H, Sun Q, Fan H. Combined exposure of alumina nanoparticles and chronic stress exacerbates hippocampal neuronal ferroptosis via activating IFN-γ/ASK1/JNK signaling pathway in rats. J Hazard Mater. 2021;411:125179.
12. Farajdokht F, Soleimani M, Mehrpouya S, Barati M, Nahavandi A. The role of hepcidin in chronic mild stress-induced depression. Neurosci Lett. 2015;588:120-4.
13. Joffe ME, Santiago CI, Oliver KH, Maksymetz J, Harris NA, Engers JL, et al. mGlu2 and mGlu3 negative allosteric modulators divergently enhance thalamocortical transmission and exert rapid antidepressant-like effects. Neuron. 2020;105(1):46-59.
14. Xiao X, Zhang H, Wang H, Li Q, Zhang T. Neuroprotective effect of amantadine on corticosterone-induced abnormal glutamatergic synaptic transmission of CA3-CA1 pathway in rat hippocampal slices. Synapse. 2017;71(12):e21993.
15. Wei S, Xu H, Xia D, Zhao R. Curcumin attenuates the effects of transport stress on serum cortisol concentration, hippocampal NO production, and BDNF expression in the pig. Domest Anim Endocrinol. 2010;39(4):231-9.
16. Chen Q, Qiu FS, Xie W, Yu WY, Su ZA, Qin GM, et al. Gypenoside A-loaded mPEG-PLGA nanoparticles ameliorate high-glucose-induced retinal microvasculopathy by inhibiting ferroptosis. Int J Pharm. 2024;666:124758.
17. Xie P, Luo HT, Pei WJ, Xiao MY, Li FF, Gu YL, et al. Saponins derived from Gynostemma pentaphyllum regulate triglyceride and cholesterol metabolism and the mechanisms: a review. J Ethnopharmacol. 2024;319:117186.
18. Dong SQ, Zhang QP, Zhu JX, Chen M, Li CF, Liu Q, et al. Gypenosides reverses depressive behavior via inhibiting hippocampal neuroinflammation. Biomed Pharmacother. 2018;106:1153-60.
19. Zhang GL, Deng JP, Wang BH, Zhao ZW, Li J, Gao L, et al. Gypenosides improve cognitive impairment induced by chronic cerebral hypoperfusion in rats by suppressing oxidative stress and astrocytic activation. Behav Pharmacol. 2011;22(7):633-44.
20. Zhang H, Wei M, Sun N, Wang H, Fan H. Melatonin attenuates chronic stress-induced hippocampal inflammatory response and apoptosis by inhibiting ADAM17/TNF-α axis. Food Chem Toxicol. 2022;169:113441.
21. Xiao J, Yao R, Xu B, Wen H, Zhong J, Li D, et al. Inhibition of PDE4 attenuates TNF-α-triggered cell death through suppressing NF-κB and JNK activation in HT-22 neuronal cells. Cell Mol Neurobiol. 2020;40(3):421-35.
22. Wang W, Wu J, Mukherjee A, He T, Wang XY, Ma Y, et al. Lysophosphatidic acid induces tumor necrosis factor-alpha to regulate a pro-inflammatory cytokine network in ovarian cancer. FASEB J. 2020;34(10):13935-48.
23. Urrutia P, Aguirre P, Esparza A, Tapia V, Mena NP, Arredondo M, et al. Inflammation alters the expression of DMT1, FPN1 and hepcidin, and it causes iron accumulation in central nervous system cells. J Neurochem. 2013;126(4):541-9.
24. Wang J, Deng B, Liu Q, Huang Y, Chen W, Li J, et al. Pyroptosis and ferroptosis induced by mixed lineage kinase 3 (MLK3) signaling in cardiomyocytes are essential for myocardial fibrosis in response to pressure overload. Cell Death Dis. 2020;11(7):574.
25. Jiang L, Kon N, Li T, Wang SJ, Su T, Hibshoosh H, et al. Ferroptosis as a p53-mediated activity during tumour suppression. Nature. 2015;520(7545):57-62.
26. Wang L, Wang H, Li L, Li W, Dong X, Li M, et al. Corticosterone induces dysregulation of iron metabolism in hippocampal neurons in vitro. Biol Trace Elem Res. 2010;137(1):88-95.
27. Zhang Z, Bai H, Ma X, Shen M, Li R, Qiu D, et al. Blockade of the NLRP3/caspase-1 axis attenuates ketamine-induced hippocampus pyroptosis and cognitive impairment in neonatal rats. J Neuroinflammation. 2021;18(1):239.

28. Duan L, Zhang Y, Yang Y, Su S, Zhou L, Lo PC, et al. Baicalin inhibits ferroptosis in intracerebral hemorrhage. Front Pharmacol. 2021;12:629379.
29. Bai L, Yan F, Deng R, Gu R, Zhang X, Bai J. Thioredoxin-1 rescues MPP(+)/MPTP-induced ferroptosis by increasing glutathione peroxidase 4. Mol Neurobiol. 2021;58(7):3187-97.
30. Roth JA, Feng L, Dolan KG, Lis A, Garrick MD. Effect of the iron chelator desferrioxamine on manganese-induced toxicity of rat pheochromocytoma (PC12) cells. J Neurosci Res. 2002;68(1):76-83.
31. Zhu Q, Gao Z, Peng J, Liu C, Wang X, Li S, et al. Lycopene alleviates chronic stress-induced hippocampal microglial pyroptosis by inhibiting the cathepsin B/NLRP3 signaling pathway. J Agric Food Chem. 2023;71(51):20034-46.
32. Shang L, Liu J, Zhu Q, Zhao L, Feng Y, Wang X, et al. Gypenosides protect primary cultures of rat cortical cells against oxidative neurotoxicity. Brain Res. 2006;1102(1):163-74.
33. Ding J, Wang BY, Yang YF, Kuai LY, Wan JJ, Zhang M, et al. Ciprofol ameliorates myocardial ischemia/reperfusion injury by inhibiting ferroptosis through upregulating HIF-1α. Drug Des Devel Ther. 2024;18:6115-32.
34. Ahmad B, Khan S, Nabi G, Gamallat Y, Su P, Jamalat Y, et al. Natural gypenosides: targeting cancer through different molecular pathways. Cancer Manag Res. 2019;11:2287-97.